INTERNATIONAL
Agrophysics
www.international-agrophysics.org

Int. Agrophys., 2025, 39, 385-398
doi: 10.31545/intagr/204531

Assessment of the early stages of rehydration observed by sorption isotherm and ^{1}H-NMR and plant growth tests for Martian regolith simulant MGS-1**

Magdalena Bacior[1]*, *Karol Kubat*[2], *Hubert Harańczyk*[2], *Monika Kula-Maximenko*[3], *Marcin Niemiec*[4], *Anna Stopka*[5], *Anna Gorczyca*[5]

[1]Department of Soil Science and Agrophysics, University of Agriculture in Kraków, Al. Mickiewicza 21, 31-120, Kraków, Poland
[2]M. Smoluchowski Institute of Physics, Jagiellonian University, S. Łojasiewicza 11, 30-348 Kraków, Poland
[3]The Franciszek Górski Institute of Plant Physiology, Polish Academy of Sciences, Niezapominajek 21, 30-239 Kraków, Poland
[4]Department of Agricultural and Environmental Chemistry, University of Agriculture in Kraków, Al. Mickiewicza 21, 31-120 Kraków, Poland
[5]Department of Microbiology and Biomonitoring, University of Agriculture in Kraków, Al. Mickiewicza 21, 31-120 Kraków, Poland

Received January 5, 2025; accepted April 29, 2025

A b s t r a c t. The early stages of gaseous phase rehydration of the Mars global simulant (MGS-1) were studied using hydration kinetics, sorption isotherm, and proton nuclear magnetic resonance (^{1}H-NMR) spectroscopy, whereas initial plant growth tests in media containing MGS-1 were assessed by microbiotests and measurement of plant biometry – seedling root length and biomass accumulation. MGS-1 is a Martian regolith analogue, whose hydration kinetics were described by a two-exponential function, and the sorption isotherm was fitted by the Dent (GAB) model. The number of empty binding sites ($1/b_1$) for humidity $h = 1$ was 1.59%, indicating the elevated hydrophobicity of the sample. The free induction decay signals (FID) were fitted by the superposition of a Gaussian component, and an exponentially decaying mobile proton signal component. The ^{1}H-NMR spectra were fitted by a Gaussian component and a narrow Lorentzian line. The NMR signal was attenuated by the presence of paramagnetic ions, particularly Fe^{2+}. A microbiotest of the initial growth of six plant species in MGS-1 mixtures with an inert substrate, *i.e.* perlite, showed high toxicity of the regolith simulant. The volumetric ratio of 2:1 (MGS-1:perlite) caused plant death and a statistically significant decrease in biomass accumulation by the tested plants. *Triticum aestivum* best tolerated the MGS-1 substrate.

K e y w o r d s: regolith, MGS-1, hydration kinetics, sorption isotherm, ^{1}H-NMR, growth of plants

*Corresponding author e-mail: magdalena.bacior@urk.edu.pl
**This work was financed by the Polish Ministry of Science and Higher Education subvention for the University of Agriculture in Krakow, Faculty of Agriculture and Economics No 010013-D011, 2025.

1. INTRODUCTION

Investigations of soil properties are especially important in the context of the effect of global warming, which has become more visible in recent decades, altering global precipitation patterns, contributing to extreme rainfall events, and long periods of drought (Ke *et al.*, 2025; Konapala *et al.*, 2020; Hugonnet *et al.*, 2021). For these reasons, arid and semi-arid areas have been expanding, with estimation that one-third of the Earth's land surface now falls into these categories (Tariq *et al.*, 2024). Experts predict that, in 2100, these dry areas could increase by an additional 4.1 and 10.6% (Liu *et al.*, 2023). This fact is a serious challenge to ecosystems, biodiversity, and agricultural productivity, especially for the soil-plant-atmosphere continuum (SPAC) (Han *et al.*, 2022; Ke *et al.* 2025).

Soil is important for producing food and raw materials for the growing world population. Hydrological processes in the soil, such as infiltration, evapotranspiration, runoff, or solute transport, affect crops. The key factor for plant growth and agricultural yields is the soil's water-holding capacity. Non-wetting soils (NWS), also known as hydrophobic or water-repellent soils, are unable to retain or allow infiltration of water to varying degrees, thereby hindering plant vegetation. NWS lack the ability to spontaneously

absorb water when water is applied to their surface (Zhu *et al.*, 2021; Majid *et al.*, 2023; Li *et al.,* 2018). Water accumulates on their surface, which limits its infiltration and significantly affects plant growth and causes soil erosion. The presence of hydrophobic organic compounds on the soil surface causes non-wetting of soils. These compounds bind to soil particles forming a coating, adhere to soil aggregates, and can occupy soil interstitial spaces (Smettem *et al.*, 2021; Zhu *et al.*, 2021). Non-wetting is a soil phenomenon occurring worldwide in various climatic conditions, in various regions, and on different soil types, except the Antarctic (Jordán *et al.*, 2013). In addition to the presence of hydrophobic compounds, many other factors induce non-wetting in soils. These factors include vegetation diversity and intensity, quality and quantity of organic matter in soils (Franco *et al.*, 1995), soil mineralogy and soil texture (Creamer *et al.*, 2019), surface area (Harper *et al.*, 2000), temperature variability associated with soil burning (Zavala *et al.*, 2009), environmental conditions, soil drying and wetting phases, humidity, drying temperature (Franco *et al.*, 1995), moisture content (Bodí *et al.*, 2013), and soil water-holding capacity. The hydrology of such soils is directly and negatively affected by reduced soil infiltration capacity and groundwater recharge. On the surface of NWS, water pools evaporate, which is especially strongly visible in dry climates, and unevenly wet the soil, often bypassing the roots of crops (Dekker *et al.*, 2001). Increased drought stress in the global climate worsens soil water repellency (SWR) (Deurer *et al.*, 2011), which contributes to delayed emergence and reduce crop growth (Li *et al.*, 2019).

In this context, our attention was focused on extraterrestrial substrates, *i.e.* the Martian regolith. The best characterised regolith on the surface of Mars is the Rocknest site within Gale Crater (Bish *et al.*, 2013; Blake *et al.*, 2013; Archer *et al.*, 2014; Achilles *et al.*, 2017; Sutter *et al.*, 2017). It consists of atmospherically dispersed dust and is therefore expected to provide a global average of the Martian regolith composition (Long-Fox and Britt, 2023). The MGS-1 standard is modelled on the wind-blown soil of Rocknest in Gale Crater, with additional information from measurements by other landed and orbiting instruments (Cannon *et al.*, 2019).

The surface of Mars is characterised by a loose and unconsolidated regolith that has been shaped by a complex interplay of processes, including impact comminution, mechanical erosion by wind, water and lava, chemical weathering by fluids and oxidants, and meteoritic impacts (Malin and Edgett, 2000; Murchie *et al.*, 2009). These processes are thought to have occurred predominantly during the early stages of Mars' history, as evidenced by the results of several studies, including those by Goetz *et al.* (2005), Yen *et al.* (2005), and Murchie *et al.* (2009). A global basaltic crust is processed into basaltic regolith, which is confirmed by remote sensing observations (McSween *et al.*, 2009; Yen *et al.*, 2005). The smallest particles, termed dust, are likely to be derived from regolith-forming processes, and represent a more "processed" and oxidised version of the subsurface. The soil composition is basaltic, as reported by Ming and Morris (2017), and is derived from a globally basaltic crust (McSween *et al.*, 2009). The Martian soil has been studied, *in situ*, at seven locations by landers and rovers, with additional data provided by orbital remote sensing (Cannon *et al.*, 2019). The major element chemistry and mineralogy of the soils at the Spirit, Opportunity, and Curiosity landing sites are similar (Yen *et al.*, 2013; Ming and Morris, 2017). This supports the hypothesis of a global basaltic soil composition (Ming and Morris, 2017), which may be locally enriched in rarer evolved volcanic compositions (*e.g.* Christensen *et al.*, 2005) or alteration phases (*e.g.* Squyres *et al.*, 2008). The Martian crust is a volcanic environment that has resulted in an igneous surface due to historic lava flows (Bridges and Warren, 2006; Hauber *et al.*, 2011). The surface consists mainly of basaltic minerals, including plagioclase feldspar, pyroxene, and silica glass (Bandfield *et al.*, 2000; Christensen *et al.*, 2000). Mars contains significant amounts of water, mainly trapped in polar ice caps (Bibring *et al.*, 2004; Lunine *et al.*, 2003). In addition, evidence for hydrated water bound to clay minerals has been found in the Martian regolith.

Actual planetary samples are often rare and expensive, making simulants a valuable alternative for research purposes. For this reason, various groups of scientists have produced 'simulants' to replicate one or more characteristics of a reference sample. These characteristics typically include the geomechanical and compositional properties of the regolith. Simulants have been used for a variety of applications, including testing engineering hardware (Bernold, 1991), conducting astrobiological studies (de Vera *et al.*, 2004), and performing plant growth experiments (Wamelink *et al.*, 2014). Scientists investigating the suitability of regolith simulants for plant growth (Wamelink *et al.*, 2014) suggest that, in addition to the chemical properties of this substrate, its water holding capacity may also be of great importance. From the point of view of substrate water management, including the possibility of plant cultivation, it has been shown that the hydrophilicity/hydrophobicity of the substrate has a clear and significant effect on the desorption/adsorption of water in the substrate and retention as well as drainage (Liu *et al.,* 2012; Zhang *et al.,* 2023). Increased soil hydrophobicity, as demonstrated by numerous studies, directly affects the reduction of water available to plants, increases surface runoff, and facilitates soil erosion. Hydrophobicity causes preferential flow, thereby increasing and contributing to groundwater pollution. It is therefore considered a highly unfavourable property of the substrate used for crops (Doerr *et al.*, 2006; Heidary *et al.*, 2018; Mielnik *et al.*, 2021).

The present paper provides a better understanding of the water binding process in the Martian regolith simulant. The hydration process of the MGS-1 simulant has been studied using hydration kinetics and sorption isotherm, which provide information on the mass of water saturating the primary water-binding sites and the hydrophilicity of the studied surface. Nuclear magnetic resonance spectroscopy was also used to differentiate the proton groups in the regolith, which differ in mobility, resulting in different values of nuclear magnetic relaxation times. The possibility of selected plants growing in the MGS-1 regolith simulant and in its mixtures with inert hydrophilic material was also initially investigated.

2. MATERIALS AND METHODS

2.1. Materials

The Mars Global Simulant (MGS-1) was purchased from Exolith Lab (USA), which provides the regolith for preliminary studies related to the concept of In-Situ Resource Utilisation (ISRU) of Mars. The MGS-1 is a third generation simulant – a mineralogical analogue of the global basaltic regolith of the Rocknest deposit from the Martian Gale crater. The basic chemical and physical properties of the simulant are presented in the publication by Cannon *et al.* (2019).

Crystalline MGS-1 phases account for 65% while the amorphous form represents the remaining 35% (wt.%).The crystalline phases include such components as plagioclase, pyroxene, olivine, magnetite, anhydrite, hematite, ilmenite, and quartz (Bish *et al.*, 2013; Achilles *et al.*, 2017), whereas the amorphous phase includes basaltic glass, hydrated silica (opal), Mg sulphate, ferrihydrate, and Fe carbonate (Cannon *et al.*, 2019). The major oxides present in the MGS-1 sample are SiO_2, FeO_T, MgO, SO_3, Al_2O_3, and CaO. The density of the MGS-1 simulant is 1.29 g cm^{-3}, which is lower than that of the original Martian basalts, for which $\rho > 3$ g cm^{-3}. This density is reduced during the physical and chemical weathering processes that form the regolith. Hydrated mineral clays have been observed on Mars as a result of the reaction of anhydrous igneous rocks with water (Ehlmann *et al.*, 2011, 2013).

2.2. Preparation of sample

The sample was stored at room temperature with a hydration level of $\Delta m/m_0 = 0.01340 \pm 0.00048$, where m_0 is the dry mass of the sample and Δm is the mass of water taken up from the gaseous phase. Prior to the hydration experiment, the air-dried sample was incubated for 168 h over silica gel ($p/p_0 = 0\%$) and dehydrated down to $\Delta m/m_0 = 0.00743 \pm 0.00013$.

The gaseous phase hydration kinetics were measured at room temperature (t = 22°C) over the surfaces of saturated solutions: LiCl (p/p_0 = 11%), CH_3COOK (p/p_0 = 23%), K_2CO_3 (p/p_0 = 43%), NH_4NO_3 (p/p_0 = 63%), $Na_2S_2O_3$ (p/p_0 = 76%), Na_2SO_4 (p/p_0 = 93%), K_2SO_4 (p/p_0 = 97%) and over the surface of water (p/p_0 = 100%) for 166 h. The dry mass of the sample was determined after heating up to 70°C for 72 h.

2.3. Statistical analysis

Before the measurements, each sample was transferred to an aluminium plate. The mass of the soil samples were determined to the nearest 0.1 mg using a WAS 220/X laboratory weighing scale. The mathematical models were analysed using OriginPro 2019 software. A chi-squared goodness of fit test was conducted for each of the tested models. The most appropriate fit was determined, and the calculations were performed to determine the values of the relevant coefficients. The significance level for all of the tests was $p<0.05$ (F-test).

2.4. Hydration kinetics

The gaseous phase hydration courses for the regolith simulant sample were fitted using the following two-exponential function:

$$\Delta m/m_0 = A_0 + A_1\left[1 - exp\left(-\frac{t}{t_1}\right)\right] + A_2\left[1 - exp\left(-\frac{t}{t_2}\right)\right], \quad (1)$$

where: t is the hydration time of the soil, $\Delta m/m_0$ is the relative mass increase, A_0 is the saturation hydration level for the fraction of tightly bound water not removed by incubation over silica gel (p/p_0 = 0%), A_1 is the saturation hydration level for the fraction of loosely bound water, t_1 is its hydration time, A_2 is the saturation hydration level for the free water fraction, and t_2 is the corresponding hydration time. The saturation hydration level for the water fraction A_2 increased gradually with increasing relative humidity.

2.5. Sorption isotherm

The total saturation hydration level, *Ch*, was calculated as the sum of all saturation hydration components:

$$Ch = \sum_{i=0}^{2} A_i, \quad (2)$$

where: A_i are the saturation hydration levels for subsequent water fractions.

The Dent (GAB) model, as a multilayer sorption model, distinguishes between two types of water binding sites, namely: (i) 'primary', directly bound to the adsorbent surface, and (ii) 'secondary', bound to primary and further bound water molecules.

The sorption isotherm for the Dent model is described by the equation:

$$\frac{\Delta m}{m_0} = Ch(h) = \frac{\Delta M}{m_0}\frac{b_1 h}{(1-bh)(1+b_1 h-bh)}, \quad (3)$$

where: h is the relative humidity (p/p_0) expressed in absolute units and $\Delta M/m_0$ is the mass of water saturating the primary water binding sites. If the number of primary water binding sites occupied by i water molecules is S_i and the

contribution of empty primary water binding sites is equal to S_0, then $S_0/S_1 = 1/b_1$. In the Dent model, the parameter b varies between 0 and 1, somehow simulating the effect of clustering. Equation (3) can be rewritten in a parabolic form Eq. (4). Both forms give the values of the parameters: $\frac{\Delta M}{m_0}$, b_1, b (Harańczyk *et al.*, 2008, 2009):

$$\frac{h}{\Delta m/m_0} = A + Bh + Ch^2. \quad (4)$$

2.6. ^{1}H-NMR experimental parameters

The ^{1}H-NMR free induction decay (FID) measurements were performed using a high power WNS HB-65 NMR relaxometer, Waterloo NMR Spectrometers (Waterloo, Ontario, Canada). The resonance frequency was 30 MHz, the main static magnetic field was B_0 = 0.7 T, the transmitter power was 400 W, the π/2 pulse length was 1.25 μs, and the repetition time was 2 s. The data were averaged over 1 000 accumulations and analysed using the CracSpin program (Węglarz and Harańczyk, 2000).

The ^{1}H-NMR spectra were recorded on a Bruker Avance III spectrometer (Bruker Biospin) operating at a resonance frequency of 300.13 MHz (at B_0 = 7 T). The transmitter power was 400 W, the pulse length π/2 = 2.2 μs, the band width was 300 kHz, and the death time was equal to 6.5 μs.

2.6.1. Measurements of ^{1}H-NMR Free Induction Decays (FIDs)

^{1}H-NMR FIDs were recorded at room temperature for the Mars Global Simulant hydrated to $\Delta m/m_0$ = 0.02, 0.03, 0.04, 0.055, 0.06, 0.08, and 0.11.

The fitted model was a superposition of the Gaussian component S and an exponentially decaying component L_1:

$$FID(t) = S\exp\left(-\left(\frac{t}{T_{2S}^*}\right)^2\right) + L_1 exp\left(-\frac{t}{T_{2L}^*}\right), \quad (5)$$

where: T_{2S}^* is the proton spin-spin relaxation time for a solid component S, taken as the time required for the Gaussian function to decay to 1/e of its initial amplitude, whereas T_{2L}^* is the effective spin-spin relaxation time of a tightly bound water fraction (L). The values of the spin-spin relaxation times have been shortened by B_0 inhomogeneities (Chavhan *et al.*, 2009).

2.6.2. Measurements of ^{1}H-NMR spectra

For the Mars Global Simulant, ^{1}H-NMR spectra were recorded at hydration levels $\Delta m/m_0$ equal to 0.02, 0.03, 0.04, 0.055, 0.06, 0.08, and 0.11.

The ^{1}H-NMR spectrum is a superposition of the Gaussian line component with the area under the line A_G coming from the solid matrix of the sample and the narrow Lorentzian line component with the area under the line A_L coming from mobile protons of the sample, most probably from the averaged fraction of bound water:

$$A(\nu) = y_0 + \frac{A_G}{\sqrt{\pi \ln 2}\Delta\nu_G}\exp\left[-2\cdot\left(\frac{\nu-\nu_G}{\sqrt{2\ln 2}\Delta\nu_G}\right)^2\right] + \frac{2A_L}{\pi}\left[\frac{\Delta\nu_L}{4(\nu-\nu_L)^2+(\Delta\nu_L)^2}\right], \quad (6)$$

where: $\Delta\nu_S$ and $\Delta\nu_L$ are the line half-widths of the Gaussian and Lorentzian components of the NMR line, ν_S and ν_L are the Gaussian and Lorentzian peak positions, and y_0 is the constant signal (equipment effect).

The proton spin-spin relaxation time of the solid component A_S can be calculated from:

$$T_{2S}^* = \frac{\sqrt{2}}{\pi\Delta\nu_S}, \quad (7)$$

where $\Delta\nu_S$ is an average value of the line half-widths of the Gaussian component for all hydration ranges.

The value of T_{2L}^* can be calculated from Eq. (8):

$$T_{2L}^* = \frac{1}{\pi\Delta\nu_L}, \quad (8)$$

where: $\Delta\nu_L$ is an average value of the line half-widths of the Lorentzian component for all hydration ranges.

2.7. Assessment of plant growth

The next aspect of the study was to assess plant growth in the Martian regolith simulant MGS-1 using the standardised PHYTOTOXKIT microbiotest in a modified form. Expanded perlite was chosen as the reference material. Perlite is a natural inert rock of volcanic origin, which is subjected to high temperature treatment after extraction, making it a homogeneous hydrophilic substrate for plant cultivation, especially in the early stages of their development. The substrate variants used in the study were the MGS-1 simulant and perlite and their volumetric mixtures in dry material proportions of 1:2 and 2:1 v:v regolith:perlite, respectively. The prepared substrates were used according to the manufacturer's instructions for the PHYTOTOXKIT microbiotest (https://www.microbiotests.com/wp-content/uploads/2019/07/phytotoxicity-test_phytotoxkit-solid-samples_standard-operating procedure.pdf), including the determination of the total water capacity, which was calculated by performing the procedure independently for all variants. Six cultivated plant species were used in the study: from the Poaceae family, the species *Triticum aestivum* (spring, *cv*. Tybalt, Malopolska HR) and *Avena sativa* (spring *cv*. Bingo, HR Strzelce); from the Fabaceae family, *Medicago sativa* (cv. Pomposa, Malopolska HR) and *Vigna radiate* (cv. Samrat); from the Brassicaceae family, *Lepidium sativum* and *Synapsis alba* (both from Phytotoxkit Package).

The direct effect of the substrates used on plant biometry and their biomass was examined in accordance with the manufacturer's procedure: filling the test plates with

substrates moistened with tap water (3 plates for each substrate variant and each plant species), placing seeds of the tested plant species, taking photos of the plates after 48 and 144 h of plant growth with a resolution of 4032x3024 pixels (72 dpi), and computer analysis of root length using the ImageJ program. The prepared plates were incubated in a phytotron in a horizontal position at 25°C for 48 h in the dark and then in a vertical position under a 12-h photoperiod with a light intensity of 220 µmol photons m^{-2} s^{-1} PPFD, and 60% RH. After 144 h of growth, the PHYTOTOXKIT plates were opened, and the plants were removed individually onto filter paper to remove excess water. The dried plants were weighed on a Radwag AS 220.R2 analytical balance with an accuracy of 0.001 mg. The obtained biometric results were statistically processed using ANOVA, and differences between the means were estimated using Tukey's HSD test at a significance level = 0.05. The results were the means of 6 replicates for each regolith:perlite combination. Data were statistically analysed using OriginPro 2020 software.

3. RESULTS AND DISCUSSION

3.1. Hydration kinetics

The air-dry sample from MGS-1 was highly dehydrated, with a hydration level of $\Delta m/m_0$ = 0.01340(48), which is a significantly lower value compared to samples from extremophilic organisms. For example, for the Antarctic lichen *Turgidosculum complicatutulum*, the value of the hydration level of the air-dry sample was equal to $\Delta m/m_0$ = 0.08, while for the Antarctic alga *Prasiola crispa* $\Delta m/m_0$ = 0.066 (Bacior *et al.*, 2017). The comparison between the MGS-1 and living organisms, such as the Antarctic lichen *Turgidosculum complicatulum* and the alga *Prasiola crispa*, highlights the significant differences in hydration levels. The Martian simulant exhibits a hydration level of $\Delta m/m_0$ = 0.01340, which is markedly lower than the values observed in these extremophiles, indicating a contrast in water retention capabilities. MGS-1 lacks biological mechanisms for hydration retention. In contrast, living organisms have evolved complex adaptations that enable them to survive in extreme conditions, *e.g.* transfer of the "freezing" loosely bound water fraction to the "non-freezing" tightly bound water fraction during the cooling down of the thallus (Bacior, 2019), as well as the presence of a "glassy state" in lichens (Carniel *et al.*, 2021).

Figure 1 shows the gaseous phase hydration courses carried out at different relative humidities (p/p_0) between 11% and 100% for MGS-1, with the recorded data expressed as the relative mass increase ($\Delta m/m_0$). The hydration kinetics were described by a two-exponential function over the whole range of humidities tested (from 11% up to 100%). Three fractions of bound water were observed, namely: (i) a fraction of tightly bound water, $\Delta m/m_0$ = 0.00527(63), and two fractions of water less bound to the surfaces of the sample, namely: (ii) a fraction of loosely bound water, $\Delta m/m_0$ = 0.00359(12), with a hydration constant of $t_1{}^h$ = 0.330(83) *h*, and (iii) a free water fraction, with a hydration constant of $t_2{}^h$ = 36.5(8.9) *h*, the amount of which increases with increasing relative humidity.

3.2. Sorption isotherm

The total saturation hydration level (Eq. (3)) at which the relative humidity *Ch* was calculated is the sum of all detected water fractions. The sorption isotherm for MGS-1 was sigmoidal in form (Fig. 2a) and was well fitted by the Dent (GAB) model. The parabolic form of the sorption isotherm is shown in Fig. 2b.

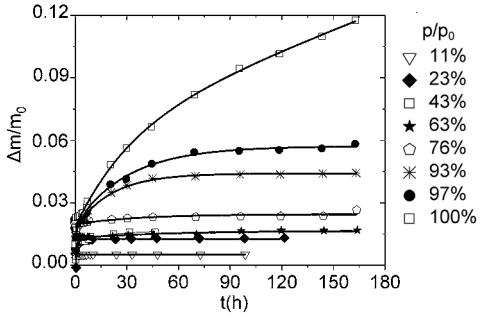

Fig. 1. Gaseous phase hydration kinetics of the MGS-1 sample recorded as a relative mass increase expressed in units of dry mass, $\Delta m/m_0$. The hydration course was performed from the gaseous phase at different values of relative humidity p/p_0. Target humidity: p/p_0: 11% – open triangles, 23% – closed diamonds, 43% – open squares, 63% – closed stars, 76% – open pentagons, 93% – stars, 97% – closed circles, 100% – open squares. The errors are within the plot symbols.

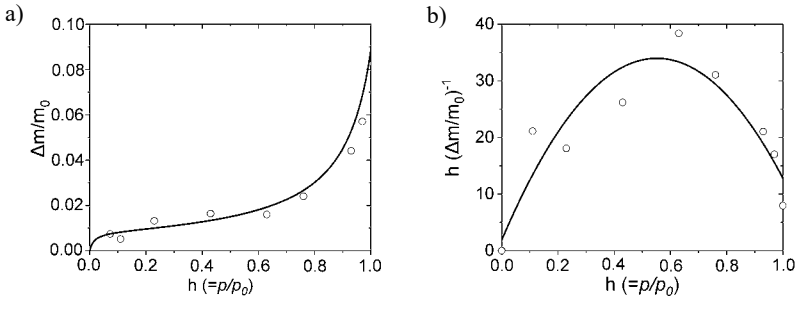

Fig. 2. a) Sorption isotherm for MGS-1 sample, b) parabolic form of the sorption isotherm.

The sorption isotherm distinguished the primary water binding sites, saturated with $\Delta M/m_0$ = 0.00837, and the secondary binding sites on the sample surface. The water mass of the monolayer is consistent with the values of the GAB model presented by Arthur *et al.* (2015). These values ranged from $\Delta M/m_0$ = 0.0014 to 0.063 for soil samples from Europe, the United States, Asia, Greenland, Africa, and South America. The mass of water saturating the primary water binding sites was much smaller than in other biological systems. For example, for extremophilic organisms from King George Island (Oceanic Antarctica), such as the Antarctic lichen *Turgidosculum complicatulum* and the alga *Prasiola crispa*, these values were equal to $\Delta M/m_0$ = 0.055 and $\Delta M/m_0$ = 0.131, respectively (Bacior *et al.*, 2017).

In the lichen *Niebla tigrina* from the Atacama Desert, this parameter was equal to 0.07 (Harańczyk, 2021). The mass of water saturating the primary binding sites was 0.086 for native starch and 0.096 for copper-modified starch (Witek, 2006). The Martian regolith simulant MGS-1 has a smaller fraction of water-binding sites than the biological systems. This means that it absorbs less water. The sum of the fractions of the tightly bound water and the loosely bound water was equal to $A_0^h + A_1^h$ = 0.0089, which is slightly higher than the fraction of water saturating the primary binding sites ($\Delta M/m_0$ = 0.00837) obtained from the Dent model.

During the hydration process, successive layers of water are attached to the surface of the tested system. If b is less than one, the Dent model is successfully applied, while the BET model is sufficient if b is equal to one (Brunauer *et al.*, 1938). The value of the parameter b from the Dent model was close to one and was equal to 0.893. This shows that the water molecules in the (n+1)-th layer cover a similar area as in the n-th layer. The obtained b value is typical for the Earth's soil samples (where b ranges from 0.53 to 0.93), while c = 70.31 for the tested MGS-1 (for Earth's soil, this value ranges from 6 to 115) (Arthur *et al.*, 2015). The number of empty water-binding sites at h = 1 was equal to $1/b_1$ = 1.59%, which means that the MGS-1 sample is more hydrophobic than native or copper-modified starch (for which $1/b_1$ = 0.1% and $1/b_1$ = 0.64%, respectively) (Witek, 2006) and comparable to extremophilic organisms. For example, for the Antarctic lichen *Cetraria aculeata* and for *Umbilicaria aprina*, this value was equal to $1/b_1$ = 0.925% and $1/b_1$ = 0.02%, respectively (Harańczyk, 2016, 2008). Higher values of empty water binding sites were observed for lyophilised DNA samples ($1/b_1$ = 2.95%) (Harańczyk, 2010) and for lyophilised dipalmitoylphosphatidylcholine (DPPC) samples, where $1/b_1$ = 11.2% (Harańczyk, 2016).

The MGS-1 regolith has a lower value of the mass of water-saturated primary water-binding sites, meaning that its surface has a lower amount of water-binding sites, *i.e.* its surface is hydrophobic. The approximate monolayer water content for 321 soil samples from different geographical origins (Arthur *et al.*, 2018) ranged from 0.0014 to 0.1002 g g^{-1} for adsorption, as calculated using the GAB model. On the other hand, the $\Delta M/m_0$ measured for 207 soil samples had values from 0.0014 to 0.063 (Arthur, 2015). The value obtained for MGS-1 samples was in the lower range of values obtained for soil samples.

Water adsorption is influenced by structural differences in various materials and organisms. The ability of extremophiles to store water is also determined by their biomolecular structure. A higher mass of water saturating primary water binding sites on the surface of Antarctic lichens plays a role in their drought and cold resistance, allowing them to maintain metabolic activity in extreme conditions. Some extremophiles contain solutes in their structure that lower the freezing point of water and enhance its retention in their cells. These adaptations are critical for survival in extreme environments with limited water availability (Harańczyk, 2003). The structural differences between extremophiles and Martian regolith simulants significantly influence their water adsorption and are crucial for understanding their potential applications in fields ranging from food science to astrobiology. Further research is needed to explore how these structural properties can be optimised for plant growth.

3.3. Measurements of ^{1}H-NMR Free Induction Decays (FIDs)

Free Induction Decay (FID) proton signals were recorded for the MGS-1 samples at hydration levels ranging from $\Delta m/m_0$ = 0.02 to 0.11 (Fig. 3). The spectra were fitted by the superposition of a Gaussian component S, originating from the solid matrix of the sample, and an exponentially relaxing mobile proton signal component L (Eq. (5)).

The spin-spin relaxation time recorded for the solid component of the MGS-1 sample (Fig. 4a) was equal to ≈ 17 μs, while the relaxation time for the mobile proton fraction L also did not change much during the hydration process and was equal to ≈ 142 μs. The MGS-1 ^{1}H-NMR FID did not distinguish between the different bound water fractions. Even in the most hydrated samples of MGS-1, the hydration level was only about 11% (Fig. 1). This was most likely due to their strong hydrophobicity. This means

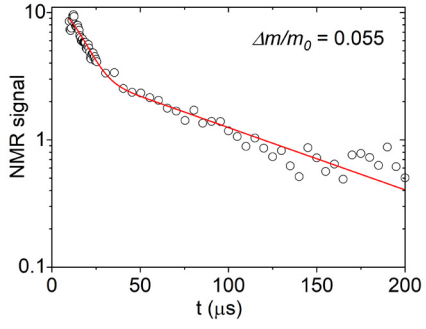

Fig. 3. FID signal recorded at room temperature for MGS-1, for the hydration level of the sample $\Delta m/m_0$ = 0.055.

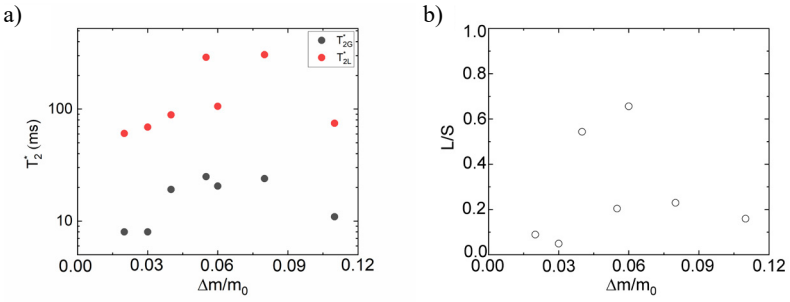

Fig. 4. a) Hydration dependence of the proton FID relaxation times for MGS-1. Solid Gaussian component S – black circles, bound water fraction L – red circles, b) L/S hydration dependence.

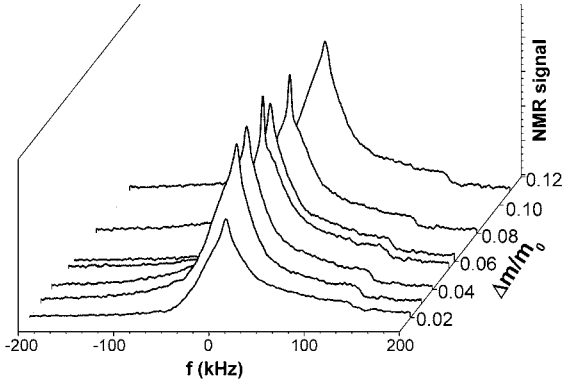

Fig. 5. Stacked plots of the ^{1}H NMR spectra measured as a function of hydration level of the MGS-1 sample hydrated to $\Delta m/m_0$ = 0.02, 0.03, 0.04, 0.055, 0.06, 0.08, and 0.11.

that only tightly bound water was present, unlike in biological systems, such as Antarctic lichen thalli (Bacior, 2017; Harańczyk, 2003; Harańczyk *et al.*, 2008, 2012).

Figure 4b shows the hydration dependence of the liquid signal amplitude expressed in units of the solid signal amplitude, *L/S*. It cannot be sufficiently fitted by a linear or rational function, as has been observed in biological systems. For example, a linear dependence was observed in the Antarctic alga *P. crispa*, while a rational function fitted well the hydration of Antarctic *T. complicatulum* or wheat seeds, suggesting the presence of a water-soluble solid fraction in these systems (Bacior *et al.*, 2017; Harańczyk *et al.*, 1996).

3.4. ^{1}H-NMR spectra

The ^{1}H NMR spectra for MGS-1 were recorded for samples hydrated in the range $\Delta m/m_0$ = 0.02 to $\Delta m/m_0$ = 0.11 (Fig. 5). The ^{1}H NMR spectra were fitted by the superposition of a Gaussian component (A_s) from the immobilised protons of the sample and a narrow Lorentzian line component (A_L) from the mobile protons of the sample. The values of the NMR signal were short, suggesting that paramagnetic ions, mainly Fe^{2+}, influence the NMR signal.

Figure 6a shows how the A_L/A_S signal changes with the hydration level of the sample. This relationship cannot be approximated by a linear or rational function, as has been observed in Antarctic organisms, such as lichens or algae. The half-widths of the broad line component for the solid matrix of MGS-1 ranged from $\Delta\nu_s$ = 90.4 kHz to $\Delta\nu_s$ = 159.7 kHz for the hydration range, increasing from $\Delta m/m_0$ = 0.02 to 0.11 (Fig. 6b). The proton spin-spin relaxation time of the solid component A_S was calculated using Eq. (7) and was equal to $T_{2S}^* \approx 3.4$ µs. This value is shorter than that observed by NMR relaxometry, for which $T_{2S}^* \approx 17$ µs for the same hydration levels of the sample. This difference is due to an additional line broadening caused by the electron paramagnetic effect and the apparatus effect.

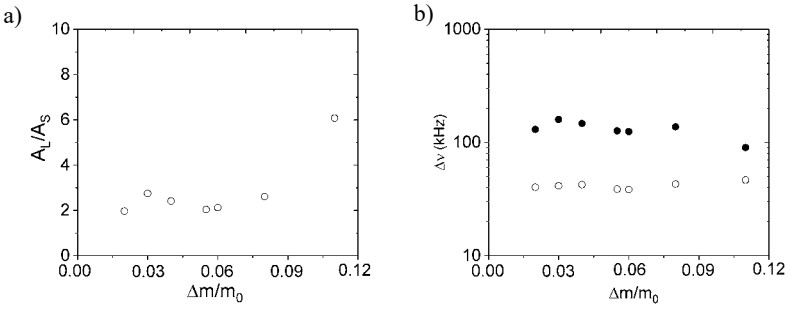

Fig. 6. a) AL/AS hydration dependence for MGS-1 sample (open circles) registered at room temperature; b) half-width of bound water (open circles) and solid Gaussian component (closed circles).

These values were smaller than those found for Antarctic organisms. For example, the spin-spin relaxation time for *Turgidosculum complicatulum* was about 19 μs from relaxometry and 12 μs from ^{1}H-NMR spectroscopy. For *Prasiola crispa* thallus, these values were 18 and 11 μs, respectively (Bacior *et al.*, 2017). The spin-spin relaxation time of the solid component was generally shorter than that of biological samples such as seeds, DNA complexes, and other lichen genera (Nizioł *et al.*, 2013; Harańczyk *et al.*, 2006).

An averaged bound water signal spectrum component was detected in the MGS-1 sample at all water contents. The half-widths (HWHM) of the solid and liquid line components did not change with water uptake (Fig. 6b). The half-widths of the Lorentzian function ranged from $\Delta\nu_L \approx$ 38.39 kHz to $\Delta\nu_L \approx$ 46.55 kHz for hydration levels from $\Delta m/m_0 = 0.02$ to 0.11.

The value of T_{2L}^* was calculated from Eq. (8). The calculated spin-spin relaxation time was equal to $T_{2L}^* \approx 7.9$ μs. This value was shorter than the average value $T_{2L}^* \approx 80$ μs registered in the time domain experiment for the tightly bound water fraction, which could be the apparatus effect caused by the presence of the paramagnetic centres in the sample.

The relaxation time obtained from NMR relaxometry ($T_{2L}^* \approx 80$ μs) is similar to that of tightly bound water in biological systems such as Antarctic lichens, photosynthetic membranes, or DNA-DDCA complexes (Harańczyk *et al.,* 2006, 2009, 2012, 2013). The fraction of loosely bound water was not detected. The position of the Gaussian and Lorentzian peaks did not change with the sample hydration level (Fig. 7).

The absence of loosely bound water in the regolith sample confirms its hydrophobic nature. Non-wetting soils have varying moisture content, which disturbs the normal growth pattern of agricultural plants (Dekker and Ritsema, 1995), particularly the germination of annual crops and pastures. A greenhouse experiment performed

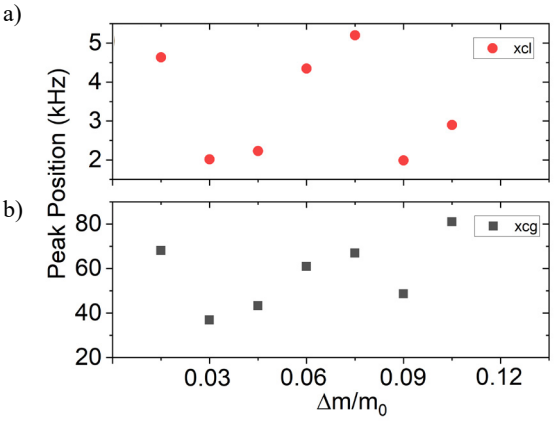

Fig. 7. Peak position of the Lorentzian a) and Gaussian b) signal as a function of hydration level of the sample.

by Chinnannan *et al.* (2024) revealed that a 75% MGS-1 concentration significantly inhibited sweet potato growth, storage root biomass, and chlorophyll content. Sweet potato exhibited optimal growth, antioxidant properties, yield, and nutrient profiles at 25% MGS-1 exposure, compared to higher concentrations.

3.5. Plant growth

Based on the characteristics specified by the regolith producer and the hydration test, it was assumed that MGS-1 would be a highly stressful substrate. The first measurement of root growth in the tested substrate mixtures showed that the MGS-1 simulant is not a substrate that allows normal plant growth. Among the species used in the study, only the roots of *V. radiata* were not statistically significantly inhibited in growth. *M. sativa*, *L. sativum*, and *T. aestivum* responded with significantly reduced root growth in the mixture with a predominance of regolith (1:2 perlite:regolith) and in regolith. The species *S. alba* and *A. sativa* were more sensitive and, even in the mixture with a lower proportion of regolith (2:1 perlite:regolith), they had significantly shorter roots compared to the growth of these plants in perlite. Figure 8 shows the results. The bioaccumulation of plant biomass assessed after 144 h of growth (Fig. 9) confirmed that MGS-1 is a substrate that inhibits the growth of the tested plants. Only *M. sativa* and *V. radiata* growing on the 1:2 mixture (regolith:perlite) produced biomass that was not statistically different from that found in the reference substrate (perlite). The remaining species already present in the substrate with such proportions showed a biomass significantly lower than that characteristic of plants growing in perlite. A very significant growth limitation in all the plants tested occurred in the mixture with a predominance of regolith. Moreover, all the species tested, except *T. aestivum*, died after 144 h. Only *T. aestivum* showed growth, but the accumulated biomass of plants from the regolith variant was almost 3 times lower than that of plants from the perlite substrate.

Considering the obtained results of plant biometry in relation to botanical families (Fig. 10), it can be stated that the roots of plants from the Fabaceae family, characterised by slow growth, showed a lower sensitivity to stress. In mixtures with a lower proportion of regolith, the Fabaceae plants did not differ significantly from those growing in perlite. However, the increased amount of regolith, and especially the regolith alone, contributed to a significant reduction in root elongation and accumulation of plant biomass. The *Brassicaceae* and *Poaceae* representatives, which showed faster growth rates, were characterised by a similar sensitivity – the substrate with a lower proportion of regolith to perlite (1:2) significantly inhibited root growth and biomass accumulation. In the substrates with the higher regolith to perlite ratio (2:1), the plant roots died and the plants were unable to accumulate biomass. Brassicaceae were more sensitive in this respect, as the

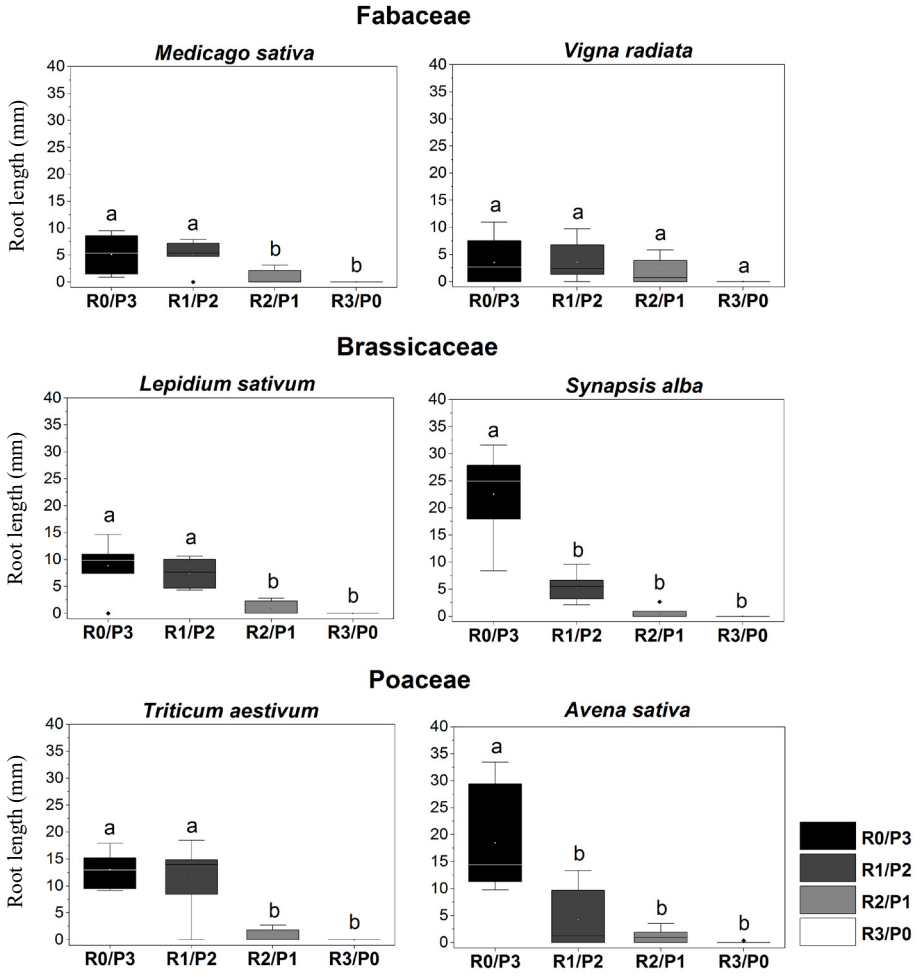

Fig. 8. Root length of tested plants species after 48 h in PHYTOTOXKIT microbiotest growth for substrate mixtures used (R0/P3 = 0:3 v:v Martian regolith simulant MGS-1:perlite; R1/P2 = 1:2 v:v Martian regolith simulant MGS-1:perlite; R2/P1 = 2:1 v:v Martian regolith simulant MGS-1:perlite; R3/P0 = 3:0 v:v Martian regolith simulant MGS-1:perlite).

plant biomass was minimal after 144 h of growth. The differences obtained can be explained by the size of the seeds (surface area in contact with the substrate), the specificity of their structure (covering, ability to swell, amount of reserve materials in the seeds, *etc*.), and the rate of seedling growth, which makes the effect of the toxic substrate more or less intense. However, it can be stated that the regolith simulant MGS-1 is a substrate with physico-chemical properties that exclude plant growth and development, even at the germination and initial seedling growth stages. This requires the development of specific techniques to treat regoliths for plant growth when planning crop cultivation related in the context of the Mars ISRU concept. Research is being carried out in this area, but the main limitation is the nature and quality of the simulants used.

The characteristics of the Martian environment are now being systematically collected by rovers and transmitted to Earth. This has allowed scientists to begin research into many aspects of ISRU, including Martian agriculture. Since the beginning of this research, it has been suggested that the correct term for the surface unconsolidated fine mineral material on planetary bodies, including Mars, is regolith, because it lacks the organic matter and microbiome that provide the basis for plant cultivation (Duri *et al.*, 2022). In addition, recent *in situ* studies have shown that the regoliths of Mars have a high salt concentration and high levels of perchlorates, which are toxic to plants. This has allowed the development and production of third-generation simulants with properties more similar to authentic regoliths, which was not possible for previous generations (Duri *et al.*, 2022).

Eichler *et al.* (2021) found that none of the composite regolith simulants available could support plant growth in the absence of nutrient supplementation, and in the case of MGS-1 (the simulant used in our study) the growth of lettuce and *Arabidopsis* was not possible even after the addition of nutrients, which the authors attributed to high alkalinity. This was confirmed by our studies of six other plant species, whose growth was limited and only possible after mixing MGS-1 with inert perlite, which alleviated the

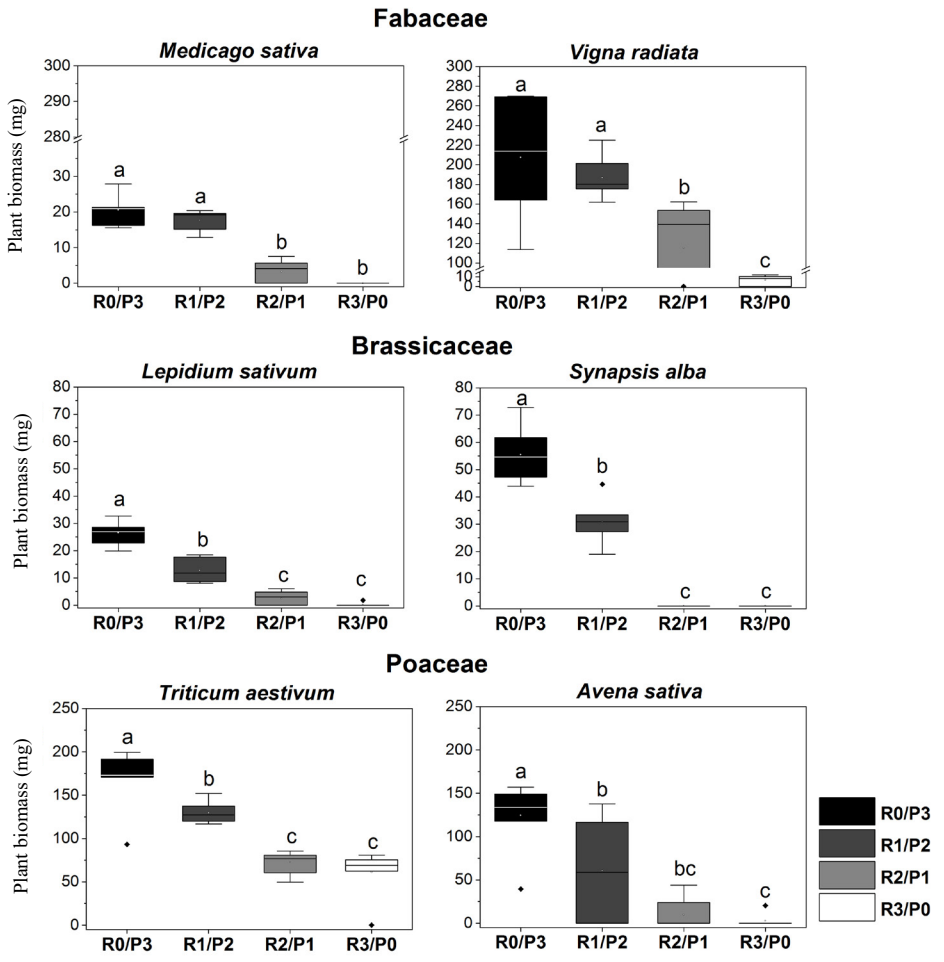

Fig. 9. Fresh biomass of a single plant after 144 h in PHYTOTOXKIT microbiotest growth for substrate mixtures used (abbreviations as for Fig. 8).

abiotic stress. Chinnannan *et al.* (2024) studied one species (sweet potato *Ipomoea batatas*) and used a method similar to ours, *i.e*. mixing MGS-1 with another substrate, garden soil rich in organic matter. The authors conclude that only a 75% garden soil admixture to MGS-1 results in optimal adaptation, strong stress tolerance, and increased yield of storage roots of the tested species.

In turn, using desert, terrestrial, and saline soils, defined as similar to Martian regolith, Ramírez *et al.* (2019) obtained growth of some potato genotypes (40% of 65 tested) and minimal yield (up to 5 g of tuber biomass per plant). The authors state that the selection of tolerant genotypes, appropriate sowing methods, and soil management strategies are crucial for crop resistance to extreme salinity. However, it has to be admitted that the yield obtained does not meet the potential food demand and further intensive research is needed on the conditioning of regolith for crop cultivation.

Wamelink *et al.* (2014, 2019) also note that, in the case of extraterrestrial agriculture, several simulant properties (alkaline pH, high sodium availability, predominance of macro compared to micro pores, low water capacity) significantly affect the possibility of plant cultivation.

The approach of mixing Martian regolith simulants with a substrate that allows plant growth provides preliminary results on the response of the studied species to the stress generated by the unfavourable properties. Our preliminary studies have shown that an important element of the planned research is the selection of the plants to be used. We have confirmed the strong toxicity of the third generation Martian regolith simulant MGS-1 for six species from three families, the need for stress mitigation to support the growth of the tested plants, and a moderate but occurring differentiation in sensitivity to the generated stress depending on the species of the tested plant.

As emphasised by Duri *et al.* (2022) in their multidisciplinary review, the ISRU approach to food production is crucial to ensure sustainability in extraterrestrial

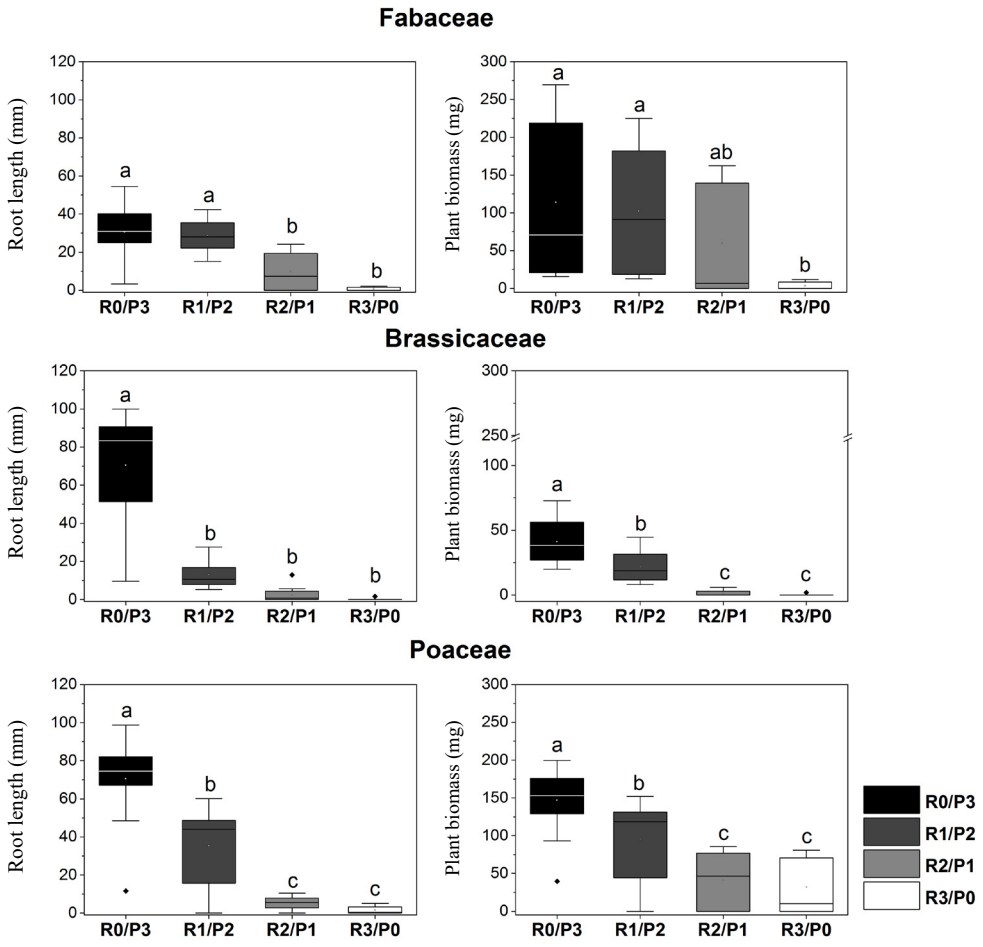

Fig. 10. Biometry (root length and fresh biomass of a single plant means) from given botanical families after 144 h in PHYTOTOXKIT microbiotest growth for substrate mixtures used (abbreviations as for Fig. 8).

settlements, and using local regolith as 'soil' for plant growth would be a feasible way to obtain food, although 'extraterrestrial soil' is very different from the vital and fertile 'terrestrial soil'. Intensive research is therefore needed to make regoliths suitable for agriculture.

4. CONCLUSIONS

The gaseous phase hydration kinetics of Martian regolith simulant MGS-1 samples were characterised by a two-exponential model. Three fractions of bound water were distinguished, namely: a tightly bound water fraction, $\Delta m/m_0 = 0.00527(63)$, which was not removed by dehydration over silica gel; a loosely bound water fraction, $\Delta m/m_0 = 0.00359(12)$, and a free water fraction, with hydration, the amount of which increased with increasing relative humidity. The MGS hydration values were shown to be lower compared even to extremophilic organisms.

The MGS-1 sorption isotherm was sigmoidal in form and was sufficiently fitted by the Dent (GAB) model. This model distinguished the primary water binding sites, which were saturated for the amount of water equal to $\Delta M/m_0 = 0.00837$. The number of empty water binding sites for humidity $h = 1$ was equal to $1/b_1 = 1.59\%$, indicating increased hydrophobicity of the sample. The Martian regolith simulant MGS-1 has structural differences from biological systems, such as lichens or algae, which significantly affect its water absorption and are critical for understanding their potential applications in extraterrestrial cultivation of plants.

Proton free induction decays (FIDs) were fitted by the superposition of a Gaussian component S from immobilised protons of the solid matrix of the sample and an exponentially relaxing mobile proton signal component L. ^{1}H NMR spectra were fitted by the superposition of a Gaussian component (A_s) from immobilised protons and a narrow Lorentzian line component (A_L) from mobile protons. The NMR signal was attenuated by the influence of paramagnetic ions (mainly Fe^{2+}) from the MGS-1 sample. The low relaxation times confirm the absence of loosely bound water in the MGS-1 as well as its hydrophobic nature. These hydrophobic properties can impact the ability of plants to grow efficiently. The study evaluating the

initial growth of plants in the MGS-1 regolith simulant confirmed that this is a substrate with properties that prevent effective plant cultivation. In the case of initial plant growth in the MGS-1 regolith simulant, it should be noted that it is a substrate with physico-chemical properties that preclude plant growth and development. The species tested, *i.e. T. aestivum*, *A. sativa* (*Poaceae*); *M. sativa*, *V. radiata* (*Fabaceae*), and *L. sativum*, *S. alba* (*Brassicaceae*) were essentially dead after 144 h of growth in the microbiotest with the MGS-1 regolith simulant.

Mixing MGS-1 with inert perlite alleviated the stress but, in substrates with a higher ratio of regolith to perlite (2:1), the plant roots died and the plants were unable to accumulate biomass. The least sensitive species tested was *T. aestivum*. Potential planning of crops within the Mars ISRU concept requires the development of complex techniques for treating extraterrestrial substrates.

Conflict of interest. The Authors declare they have no conflict of interest.

5. REFERENCES

Achilles, C.N., Downs, R.T., Ming, D.W., Rampe, E.B., Morris, R.V., Treiman, A.H., *et al.*, 2017. Mineralogy of an active eolian sediment from the Namib dune, Gale crater. Mars. J. Geophys. Res. 112, 2344-2361. https://doi.org/10.1002/2017JE005262

Archer, Jr. P.D., Franz, H.B., Sutter, B., Arevalo, Jr. R.D., Coll, P., Eigenbrode, J.L., *et al.*, 2014. Abundances and implications of volatilebearing species from evolved gas analysis of the Rocknest Aeolian deposit, Gale Crater, Mars. J. Geophys. Res. 119, 237-254. https://doi.org/10.1002/2013JE004493

Arthur, E., Tuller, M., Moldrup, P., de Jonge, L.W., 2015. Evaluation of theoretical and empirical water vapor sorption isotherm models for soils. Water Resour. Res. 55, 190-205. https://doi.org/10.1002/2015WR017681

Arthur, E., Tuller, M., Moldrup, P., Greve, M.H.M. Knadela, de Jonge, L.W., 2018. Applicability of the Guggenheim Anderson Boer water vapour sorption model for estimation of soil specific surface area. European J. Soil Sci. 69, 245-255. https://doi: 10.1111/ejss.12524

Bacior, M., Harańczyk, H., Nowak, P., Kijak, P., Marzec, M., Fitas, J., Olech, M.A., 2019. Low-temperature immobilization of water in Antarctic Turgidosculum and in *Prasiola crispa*. Part I. *Turgidosculum complicatulum*. Biointerfaces 173, 869-875. https://doi.org/10.1016/j.colsurfb.2018.10.059

Bacior, M., Nowak, P., Harańczyk, H., Patryas, S., Kijak, P., Ligęzowska, A., *et al.*, 2017. Extreme dehydration observed in Antarctic *Turgidosculum complicatulum* and in *Prasiola crispa*. Extremophiles 21, 331-343. https://doi.org/10.1007/s00792-016-0905-z

Bandfield, J.L., Hamilton, V.E., Christensen, P.R., 2000. A global view of Martian surface compositions from MGS-TES. Science 287, 1626-1630. https://doi.org/10.1126/science.287.5458.1626

Bernold, L.E., 1991. Experimental studies on mechanics of lunar excavation. J. Aerosp. Eng. 4, 9. https://doi.org/10.1061/(ASCE)0893-1321(1991)4:1(9)

Bibring, J.P., Langevin, Y., Poulet, F., Gendrin, A., Gondet, B., Berthé M., *et al.*, 2004. Perennial water ice identified in the south polar cap of Mars. Nature 428, 627-630. https://doi.org/10.1038/nature02461

Bish, D.L., Blake, D.V., Vaniman, D.T., Chipera, S.J., Morris, R.V., Ming, D.W., *et al.*, 2013. X-ray diffraction results from Mars science laboratory: mineralogy of rocknest at Gale Crater. Science 341, 1238932. https://doi.org/10.1007/978-1-4614-6339-9_12

Blake, D.F., Morris, R.V., Kocurek, G., Morrison, S.M., Downs, R.T., Bish, D., *et al.*, 2013. Curiosity at Gale Crater, Mars: characterization and analysis of the rocknest sand shadow. Science 341, 1239505.

Bodí, M.B., Munoz-Santa, I., Armero, C., Doerr, S.H., Mataix-Solera, J., Cerdà, A., 2013. Spatial and temporal variations of water repellency and probability of its occurrence in calcareous Mediterranean rangeland soils affected by fires. Catena 108, 14-25. https://doi.org/10.1016/j.catena.2012.04.002

Bridges, J.C., Warren, P.H., 2006. The SNC meteorites: basaltic igneous processes on Mars. J. Geol. Soc. 163, 229-251. https://doi.org/10.1144/0016-764904-501

Brunauer, S., Emmett, P.H., Teller, E. 1938. Adsorption of gases in multimolecular layers. J. Am. Chem. Soc. 60, 309-319. https://doi.org/10.1021/ja01269a023

Cannon, K.M., Britt, D.T., Smith, T.M., Fritsche, R.F., Batcheldor, D., 2019. Mars global simulant MGS-1: A Rocknest-based open standard for basaltic martian regolith simulants. Icarus 317, 470-478. https://doi.org/10.1016/j.icarus.2018.08.019

Carniel, F.C., Fernandez-Marín, B., Arc, E., Craighero, T., Laza, J.M., Incerti, M.G., Tretiach, M., Kranner I., 2021. How dry is dry? Molecular mobility in relation to thallus water content in a lichen. J. Exp. Bot. 72, 1576-1588. https://doi.org/10.1093/jxb/eraa521

Chavhan, G.B., Babyn, P.S., Thomas, B., Shroff, M.M., Haacke, E.M., 2009. Principles, techniques, and applications of T2*-based MR imaging and its special applications. Radiographics 29, 1433-1449. https://doi.org/10.1148/rg.295095034

Chinnannan, K., Somagattu, P., Yammanuru, H., Nimmakayala, P., Chakrabarti, M., Reddy, U.K., 2024. Effects of Mars Global Simulant (MGS-1) on growth and physiology of sweet potato: A space model plant. Plants 13(1), 55. https://doi.org/10.3390/plants13010055

Christensen, P.R., Bandfield, J.L., Smith, M.D., Hamilton, V.E., Clark, R.N., 2000. Identification of a basaltic component on the Martian surface from Thermal Emission Spectrometer data. J. Geophys. Res. 105, 9609-9621. https://doi.org/10.1029/1999JE001127

Christensen, P.R., McSween, Jr. H.Y., Bandfield, J.L., Ruff, S.W., Rogers, A.D., Hamilton, V.E., *et al.*, 2005. Evidence for magmatic evolution and diversity on Mars from infrared observations. Nature 436, 504-509. https://doi.org/10.1038/nature03639

Creamer, C.A., Foster, A.L., Lawrence, C., McFarland, J., Schulz, M., Waldrop, M.P., 2019. Mineralogy dictates the initial mechanism of microbial necromass association. Geochim. Cosmochim. Acta 260, 161-176. https://doi.org/10.1016/j.gca.2019.06.028

Dekker L.W., Doerr S.H., Oostindie K., Ziogas A.K., Ritsema, C.J., 2001. Water Repellency and Critical Soil Water Content in a Dune Sand. Soil Sci. Soc. Am. J. 65, 1667-1674. https://doi.org/10.2136/sssaj2001.1667

Dekker, L.W., Ritsema, C.J., 1995. Fingerlike Wetting Patterns in Two Water-Repellent Loam Soils. J. Environ. Qual. 24, 324-333. https://doi.org/10.2134/jeq1995.00472425002400020016x

Deurer, M., Müller, K., van den Dijssel, C., Mason, K., Carter, J., Clothier, B.E., 2011. Is soil water repellency a function of soil order and proneness to drought? A survey of soils under pasture in the North Island of New Zealand. Eur. J. Soil Sci. 62, 765-779. https://doi.org/10.1111/j.1365-2389.2011.01392.x

de Vera, J.-P., Horneck, G., Rettberg, P., Ott, S., 2004. The potential of the lichen symbiosis to cope with the extreme conditions of outer space II: germination capacity of lichen ascospores in response to simulated space conditions. Adv. Space Res. 33, 1236-1243. https://doi.org/10.1016/j.asr.2003.10.035

Doerr, S.H., Shakesby, R.A., Dekker, L.W., Ritsema, C.J., 2006. Occurrence, prediction and hydrological effects of water repellency amongst major soil and land-use types in a humid temperate climate. Eur. J. Soil Sci. 57(5), 741-754. https://doi.org/10.1111/j.1365-2389.2006.00818.x

Duri, L.G., Caporale, A.G., Rouphael, Y., Vingiani, S., Palladino, M., De Pascale, S., Adamo, P., 2022. The potential for lunar and martian regolith simulants to sustain plant growth: a multidisciplinary overview. Front. Astron. Space Sci. 8. https://doi.org/10.3389/fspas.2021.747821

Ehlmann, B.L., Berger, G., Mangold, N., Michalski, J.R., Catling, D.C., Ruff, S.W., *et al.*, 2013. Geochemical consequences of widespread clay mineral formation in Mars' ancient crust. Space Sci. Rev. 174, 329-364. https://doi.org/10.1007/978-1-4614-7774-7_11

Ehlmann, B.L., Mustard, J.F., Murchie, S.L., Bibring, J.-P., Meunier, A., Fraeman, A.A., *et al.*, 2011. Subsurface water and clay mineral formation during the early history of Mars. Nature 479, 53-60. https://doi.org/10.1038/nature10582

Eichler, A., Hadland, N., Pickett, D., Masaitis, D., Handy, D., Perez, A., Batcheldor, D., Wheeler, B., Palmer, A., 2021. Challenging the agricultural viability of martian regolith simulants, Icarus 354, 114022. https://doi.org/10.1016/j.icarus.2020.114022

Franco, C., Tate, M., Oades, J., 1995. Studies on non-wetting sands.1. The role of intrinsic particulate organic-matter in the development of water-repellency in non-wetting sands. Soil Res. 33, 253-263. https://doi.org/10.1071/SR9950253

Goetz, W., Bertelsen, P., Binau, C.S., Gunnlaugsson, H.P., Hviid, S.F., Kinch, K.M., *et al.*, 2005. Indication of drier periods on Mars from the chemistry and mineralogy of atmospheric dust. Nature 436, 62-65. https://doi.org/10.1038/nature03807

Han, J., Zhang, J., Yang, S., Cao, D., Prodhan, F.A., Sharma, T.P., 2022. A new composite index for global soil plant atmosphere continuum drought monitoring combing remote-sensing based terrestrial water storage and vapor pressure deficit anomalies. J. Hydrol. 615, 128622. https://doi.org/10.1016/j.jhydrol.2022.128622

Harańczyk, H., 2003. On water in extremely dry biological systems. Jagiellonian University, Kraków, 2003.

Harańczyk, H., Czak, J., Nowak, P., Nizioł, J., 2010. Initial phases of DNA rehydration by NMR and sorption isotherm. Acta Physica Polonica A, 117, 397-402. https://doi.org/10.12693/APhysPolA.117.397

Harańczyk, H., Bacior, M., Olech, M., 2008. Deep dehydration of Umbilicaria aprina thalli observed by proton NMR and sorption isotherm. Antarct. Sci. 20(6), 527-535. https://doi.org/10.1017/S0954102008001363

Harańczyk, H., Bacior, M., Jastrzębska, P., Olech, M.A., 2009. Deep dehydration of Antarctic lichen Leptogium puberulum Hue observed by NMR and sorption isotherm. Acta Phys. Pol. A, 115, 516-520. https://doi.org/10.12693/APhysPolA.115.516

Harańczyk, H., Kobierski, J., Nizioł, J., Hebda, E., Pielichowski, J., Zalitacz, D., *et al.*, 2013. Mild hydration of didecyldimethylammonium chloride modified DNA by 1H-nuclear magnetic resonanc, e and by sorption isotherm. J. App. Phys. 113, 044702. https://doi.org/10.1063/1.4789011

Harańczyk, H., Kobierski, J., Zalitacz, D., Nowak, P., Romanowicz, A., Marzec, M., *et al.*, 2012. Rehydration of CTMA modified DNA powders observed by NMR. Acta Phys. Pol. A, 121, 485-490. https://doi.org/10.12693/APhysPolA.121.485

Harańczyk, H., Leja, A., Strzałka, K., 2006. The effect of water accessible paramagnetic ions on subcellular structures formed in developing wheat photosynthetic membranes as observed by NMR and by sorption isotherm. Acta Phys. Pol. A, 109, 389-398. https://doi.org/10.12693/APhysPolA.109.389

Harańczyk, H., Strzałka, K., Jasiński, G., Mosna-Bojarska, K., 1996. The initial stages of wheat (*Triticum aestivum* L.) seed imbibition as observed by proton nuclear magnetic relaxation. Colloids Surf. A: Physicochem. Eng. Asp., 115, 47-54. https://doi.org/10.1016/0927-7757(96)03615-1

Harper, R.J., McKissock, I., Gilkes, R.J., Carter, D.J., Blackwell, P.S., 2000. A multivariate framework for interpreting the effects of soil properties, soil management and landuse on water repellency. J. Hydrol. 231-232, 371-383. https://doi.org/10.1016/S0022-1694(00)00209-2

Hauber, E., Brož, P., Jagert, F., Jodłowski, P., Platz, T., 2011. Very recent and wide-spread basaltic volcanism on Mars. Geophys. Res. Lett. 38, L10201. https://doi.org/10.1029/2011GL047310

Heidary, K., Najafi, Nejad, A., Dekker, L., Ownegh, M., Mohammadian Behbahani, A., 2018. Impact of soil water repellency on hydrological and erosion processes; a review. Ecopersia 6(4), 269-284.

Hugonnet, R., McNabb, R., Berthier, E., Menounos, B., Nuth, C., Girod, L., Farinotti, D., Huss, M., Dussaillant, I., Brun, F., Kääb, A., 2021. Accelerated global glacier mass loss in the early twenty-first century. Nat. Clim. Change 592, 726-731. https://doi.org/10.1038/s41586-021-03436-z

Jordán, A., Zavala, L.M., Mataix-Solera, J., Doerr, S.H., 2013. Soil water repellency: origin, assessment and geomorphological consequences. Catena 108, 1-5. https://doi.org/10.1016/j.catena.2013.05.005

Ke, X., Yao, J., Jiang, Z., Gu, X., Xu, P., 2025. Recover and surpass: The mechanisms of plants transition upon rehydration from drought. Plant Stress 15, 100782. https://doi.org/10.1016/j.stress.2025.100782

Konapala, G., Mishra, A.K., Wada, Y., Mann, M.E., 2020. Climate change will affect global water availability through compounding changes in seasonal precipitation and evaporation. Nat. Commun. 11, 3044. https://doi.org/10.1038/s41467-020-16757-w

Li, Y., Yao, N., Tang, D., Chau, H. W., Feng, H., 2019. Soil water repellency decreases summer maize growth. Agric. For. Meteorol. 266-267, 1-11. https://doi.org/10.1016/j.agrformet.2018.12.001

Li, Y., Ren, X., Hill, R., Malone, R., and Zhao, Y., 2018. Characteristics of Water Infiltration in Layered Water-Repellent Soils. Pedosphere 28, 775-792. https://doi.org/10.1016/S1002-0160(17)60414-4

Liu, H., Ju, Z., Bachmann, J., Horton, R., Ren, T., 2012. Moisture-dependent wettability of artificial hydrophobic soils and its relevance for soil water desorption curves. Soil Sci. Soc. Am. J. 76(2), 342-349. https://doi.org/10.2136/sssaj2011.0081

Liu, K., Li, X., Wang, S., Zhou, G., 2023. Past and future adverse response of terrestrial water storages to increased vegetation growth in drylands. npj Clim. Atmos. Sci. 6, 113. https://doi.org/10.1038/s41612-023-00437-9

Long-Fox, J.M., Britt, D.T., 2023. Characterization of planetary regolith simulants for the research and development of space resource technologies. Front. Space Technol. 4: 1255535. https://doi.org/10.3389/frspt.2023.1255535

Lunine, J.I., Chambers, J., Morbidelli, A., Leshin, L.A., 2003. The origin of water on Mars. Icarus 165, 1-8. https://doi.org/10.1016/S0019-1035(03)00172-6

Majid, N., Bahar, M., Harper, R. Megharaj, M., Naidu, R., 2023. Influence of biotic and abiotic factors on the development of non-wetting soils and management approaches. Soil Security 11, 100091. https://doi.org/10.1016/j.soisec.2023.100091

Malin, M.C., Edgett, K.S., 2000. Sedimentary rocks of early Mars. Science 290, 1927-1937. https://doi.org/10.1126/science.290.5498.1927

McSween, Jr. H.Y., Taylor, G.J., Wyatt, M.B., 2009. Elemental composition of the Martian crust. Science 324, 736-739. https://doi.org/10.1126/science.1165871

Mielnik, L., Hewelke, E., Weber, J., Oktaba, L., Jonczak, J., Podlasiński, M., 2021. Changes in the soil hydrophobicity and structure of humic substances in sandy soil taken out of cultivation. Agric. Ecosyst. Environ. 319, 107554. https://doi.org/10.1016/j.agee.2021.107554

Ming, D.W., Morris, R.V., 2017. Chemical, mineralogical, and physical properties of Martian dust and soil. In: Dust in the Atmosphere of Mars and Its Impact on Human Exploration. Ed.: Levine, J.S., Winterhaler, D., Kerschmann, R.L. Cambridge Scholars Publishing, UK.

Murchie, S.L., Mustard, J., Ehlmann, B.L., Milliken, R.E., Bishop, J.L., McKeown, N.K., *et al.*, 2009. A synthesis of Martian aqueous mineralogy after 1 Mars year of observations from the Mars Reconnaissance Orbiter. J. Geophys. Res. 114, E00D06. https://doi.org/10.1029/2009JE003342

Nizioł, J., Harańczyk, H., Kobierski, J., Hebda, E., Pielichowski, J., Ostachowicz, B., 2013. Hydration effect on solid DNA-didecyldimethylammonium chloride complexes measured using H-nuclear magnetic resonance spectroscopy. J. Appl. Phys. 114, 144701. https://doi.org/10.1063/1.4824374

Ramírez, D.A., Kreuze, J., Amoros, W., Valdivia-Silva, J.E., Ranck, J., Garcia, S., Salas, E., Yactayo, W., 2019. Extreme salinity as a challenge to grow potatoes under mars-like soil conditions: targeting promising genotypes. Int. J. Astrobiol. 18, 18-24. https://doi.org/10.1017/S1473550417000453

Smettem, K.R.J., Rye, C., Henry, D.J., Sochacki, S.J., Harper, R.J., 2021. Soil water repellency and the five spheres of influence: a review of mechanisms, measurement and ecological implications. Sci. Total Environ. 787, 147429. https://doi.org/10.1016/j.scitotenv.2021.147429

Squyres, S.W., Arvidson, R.E., Ruff, S., Gellert, R., Morris, R.V., Ming, D.W., *et al.*, 2008. Detection of silica-rich deposits on Mars. Science 320, 1063-1067. https://doi.org/10.1126/science.1155429

Sutter, B., McAdam, A.C., Mahaffy, P.R., Ming, D.W., Edgett, K.S., Rampe, E.B., *et al.*, 2017. Evolved gas analyses of sedimentary rocks and eolian sediment in Gale Crater, Mars: results of the curiosity rover's sample analysis at Mars (SAM) instrument from Yellowknife Bay to the Namib Dune. J. Geophys. Res. 122, 2564-2609. https://doi.org/10.1002/2016JE005225

Tariq, A., Sardans, J., Zeng, F., Graciano, C., Hughes, A.C., Farré-Armengol, G., Peñuelas, J., 2024. Impact of aridity rise and arid lands expansion on carbon-storing capacity, biodiversity loss, and ecosystem services. Glob. Chang. Biol. 30, e17292. https://doi.org/10.1111/gcb.17292

Wamelink, G.W.W., Frissel, J.Y., Krijnen, W.H.J., Verwoert, M.R. 2019. Crop growth and viability of seeds on Mars and Moon soil simulants. Open Agric. 4, 509-516. https://doi.org/10.1515/opag-2019-0051

Wamelink, G.W.W., Frissel, J.Y., Krijnen, W.H.J., Verwoert, M.R., Goedhart, P.W., 2014. Can plants grow on Mars and the Moon: A growth experiment on Mars and Moon soil simulants. PLoS One 9, e103138. https://doi.org/10.1371/journal.pone.0103138

Węglarz, W., Harańczyk, H., 2000. Two-dimensional analysis of the nuclear relaxation function in the time domain: the program CracSpin. J. Phys. D: Appl. Phys. 33, 1909-192. https://doi.org/10.1088/0022-3727/33/15/322

Witek, M., Peemoeller, H., Szymońska, J., Blicharska, B., 2006. Investigation of Starch Hydration by 2D Time Domain NMR. Acta Phys. Pol. 3, 359-364. https://doi.org/10.12693/APhysPolA.109.359

Yen, A.S., Gellert, R., Clark, B.C., Ming, D.W., King, P.L., Schmidt, M.E., *et al.*, 2013. Evidence for a global martian soil composition extends to Gale Crater. In: Proceedings of the Lunar and Planetary Science Conference, XLIV, 44 Abstract #2495.

Yen, A.S., Gellert, R., Schröder, C., Morris, R.V., Bell, III, J.F., Knudson, A.T., *et al.*, 2005. An integrated view of the chemistry and mineralogy of martian soils. Nature 436, 49-54. https://doi.org/10.1038/nature03637

Zavala, L.M., González, F.A., Jordán, A., 2009. Intensity and persistence of water repellency in relation to vegetation types and soil parameters in Mediterranean SW Spain. Geoderma 152, 361-374. https://doi.org/10.1016/j.geoderma.2009.07.011

Zhang, Q., Chen, W., Chu, J., 2023. Effect of soil hydrophobicity on soil-water retention curve of a silt loam soil. Soil Till. Res. 234, 105855. https://doi.org/10.1016/j.still.2023.105855

Zhu, P., Zhang, G., Wang, H., Zhang, B., Liu, Y., 2021. Soil moisture variations in response to precipitation properties and plant communities on steep gully slope on the Loess Plateau. Agric. Water Manag. 256, 107086. https://doi.org/10.1016/j.agwat.2021.107086